Publication in the journal 'Oxidation of Metals' (Peer-reviewed)

Steam Oxidation Evaluation of Fe-Cr Alloys for Accident Tolerant Nuclear Fuel Cladding

B. A. Pint and K. A. Unocic

Oak Ridge National Laboratory, P.O. Box 2008, Oak Ridge, TN 37831-6156 USA

Abstract. New nuclear fuel cladding materials are being evaluated that can withstand steam environments ≥1200°C for short (≤4 h) periods in case of a beyond design basis accident. This study focused on commercial and model Fe-Cr alloys, where there is considerable experience in fabricating and joining. Exposures in 1 bar steam and air for 4 h at 800°-1200°C showed that the commercial Fe-Cr alloys were very sensitive to composition and only Fe-25.8%Cr-1%Mo alloy formed a protective chromia scale at 1200° and 1300°C in steam. A model Fe-22.5%Cr+Mn,Si,Y alloy also formed a protective scale at 1200°C in steam. Analytical transmission electron microscopy of the reaction products revealed that (1) nominally equiaxed Cr_2O_3 formed at 1000°-1200°C, (2) at 1000°C, there was a Mn inner and outer layer but at 1100° and 1200°C only an outer layer was observed; (3) an amorphous SiO_2 inner layer was observed at 1000° and 1100°C but the SiO_2 was crystalline on the 22.5%Cr model alloy at 1200°C, which was confirmed by electron and x-ray diffraction and (4) Fe was found throughout the Cr_2O_3 formed without Mn at 1200°C in steam and air; oxide near the gas interface and Fe-rich metal precipitates near the metal-oxide interface. A few Fe-rich precipitates were detected in oxides formed at 1100°C and none at 1000°C. The incorporation of Fe and crystallization of SiO_2 at 1200°C may be detrimental to the formation of a protective chromia scale in steam at ≥1200°C for this application.

Keywords: Nuclear Energy, Fuel Cladding, Steam Oxidation, FeCr Alloys

INTRODUCTION

The nuclear accident in Japan in March 2011 focused attention on the performance of nuclear fuel cladding during severe accident conditions [1]. Current light water reactors typically use UO_2 fuel rods with Zr-based fuel cladding [2,3]. However, when the water level drops in the reactor during a severe accident, the heat of Zr oxidation contributes to the temperature increase in the reactor and the hydrogen generated contributed to the 2011 disaster. To provide larger safety margins during a future accident [4], a selection metric has been established to identify materials that oxidize ≥100X slower than Zr at 1200°C in steam [5,6], while retaining reasonable neutronics performance (e.g. high Ni contents are unacceptable) [3,5]. Thus, candidates such as SiC, FeCr, FeCrAl and MAX phases have been evaluated in steam oxidation at 800°-1500°C for this application [6-11], with considerable interest in FeCrAl [12], which can retain steam oxidation resistance to 1500°C [11]. However, FeCrAl alloys can suffer from low ductility and difficulty in joining and fabrication of thin-walled (<0.4mm) cladding.

A more traditional choice is FeCr alloys. The oxidation resistance of FeCr alloys has been extensively studied for more than 50 years [13-27], including studies up to 1200°C when it was considered in the 1970's as a possible skin of the U.S. space shuttle. Steam oxidation, including the effect of water vapor, has mainly been studied at 500°-800°C where FeCr (or FeCrNi) alloys might be used in structural applications. However, the steam oxidation behavior at 1000°-1200°C has not been evaluated in most cases. A few model Fe-Cr alloys were studied previously for this accident tolerant fuel (ATF) cladding application with the conclusion that ~25%Cr was needed for steam oxidation resistance at 1200°C [8-9]. In this study, a range of commercial Fe-Cr alloys were evaluated in steam oxidation with three selected with ~25%Cr. For comparison, several model alloys were included to help understand the role of composition on performance. The commercial alloys were surprisingly sensitive to Cr content and characterization of the reaction

products using analytical scanning transmission electron microscopy (STEM) helped understand the observed performance.

EXPERIMENTAL PROCEDURE

Specimens evaluated in this study were coupons typically ~1.5x10x20 mm with compositions given in Table I in mass % and a 600 grit polish. The model FeCr alloys (i.e. F22MSY, F25MSY, F25N) were cast at Oak Ridge National Laboratory (ORNL) followed by hot rolling and annealing at 1100°C. Oxidation experiments were conducted for 4 h at 800°-1300°C in a magnetic suspension thermal gravimetric analysis instrument (Rubotherm model DynTHERM LP-HT-II) where the alumina test chamber was fully isolated from the environment of dry air or 100% steam flowing at 1-2 cm/s [11]. The specimens were suspended with a Pt-Rh wire. The deionized water used to generate steam was not Ar-bubbled or filtered as is typically done for ~600°C testing because the equilibrium O_2 content in steam at 1200°C is much higher than at low temperature [6]. The mass change of all specimens was checked using a Mettler Toledo model XP205 balance with ±0.04 mg or ±0.01 mg/cm2 accuracy. After exposure, specimens were metallographically sectioned and examined by light microscopy and x-ray diffraction using a Panalytical X'pert Pro diffractometer with Mo Kα radiation. The STEM specimens were prepared using the focused ion beam (FIB) lift out technique and imaging was carried out using a FEI model Talos F200X STEM with an integrated energy dispersive x-ray system with four silicon drift detectors.

RESULTS

Figure 1a summarizes the mass change data for the six commercial alloys as a function of temperature. Typically 5-6 experiments were conducted for each alloy depending on where the alloy showed protective behavior, i.e. low mass change. At each temperature where the alloy was exposed in 1 bar steam, a corresponding exposure was conducted in dry air in order to determine the effect of steam on the oxidation behavior of these alloys. For Grade 91, a high mass gain was observed in steam at 800°, 900° and 1000°C. In contrast, protective behavior was observed in air at 800°C but not at higher temperatures. Both the 405 and 430 specimens showed a low mass gain at 800°C in steam but a higher mass gain at 900°C. In air, protective behavior was observed at 900°C for both alloys with a much higher mass gain observed after exposure at 1000°C. The higher Cr content alloys were evaluated at 1000°-1200°C. The 446 specimen was not protective at 1100°C in steam, while the 4C54 specimen was not protective at 1200°C in steam. EBrite showed protective behavior at both 1200° and 1300°C in steam. Figure 1b summarizes the maximum temperature capability of each of the alloys as a function of alloy Cr content illustrating how sensitive the maximum temperature was to alloy Cr content. The mass change data for the model alloys is not shown in Figure 1a for clarity but the performance is shown in Figure 1b.

Figure 2 shows examples of the thin reaction products formed corresponding to the low mass gains in Figure 1a. The commercial steels in this study tended to have low Al and Ti contents (Table 1) and thus little or no internal oxidation, except for silica that formed beneath the Cr-rich scale at 1100° and 1200°C. The model F25N specimen showed obvious evidence of void formation, Figure 2f. In Figures 2d-2e, it is difficult to differentiate silica formation from possible void formation at the metal-scale internface. X-ray diffraction showed that the oxides formed on the steels were typically α-Cr_2O_3 with indications of Mn and Fe incorporation.

Table 1. Chemical composition of the alloys measured by inductively coupled plasma and combustion analyses.

Alloy	Fe	Cr	Mn	Si	Al	Ti	N	S	Other
Gr.91	88.7	9.1	0.39	0.24	<	<	0.052	0.0122	0.86Mo,0.1Cu,0.1Nb,0.1V
405	85.8	12.9	0.48	0.37	0.26	0.003	0.023	<0.0003	0.1Ni
430	82.1	16.7	0.49	0.26	0.004	0.002	0.031	0.0009	0.2Ni
446	73.4	24.9	0.76	0.19	<	0.003	0.108	0.0098	0.2Ni,0.1V
4C54	72.5	25.4	0.71	0.49	<	0.004	0.166	0.0036	0.3Ni,0.1V
EBrite	72.6	25.8	<	0.22	<	<	0.008	0.0100	1.0Mo,0.1Ni.0.1V,0.1Nb
F22MSY	76.6	22.5	0.23	0.71	0.01	<	0.0012	0.0029	0.0016Y
F25MSY	74.0	25.0	0.67	0.25	0.01	<	0.0008	0.0030	0.0019Y
F25N	74.3	25.6	<	0.015	<	<	0.0008	0.0020	0.04O

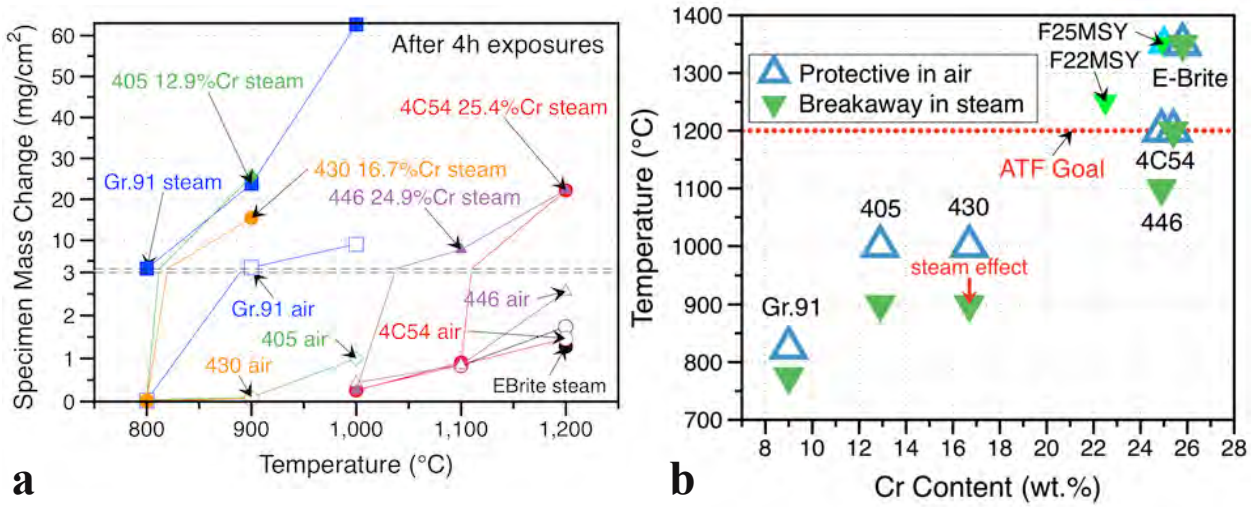

FIGURE 1. (a) Specimen mass change data after 4h exposures in air or steam as a function of exposure temperature, and (b) steam and air temperature limits for the FeCr alloys as a function of Cr content. The dashed line in (b) shows the ATF cladding goal of steam oxidation resistance at a minimum of 1200°C.

Figure 3 shows examples of the thick Fe-rich oxides formed, consistent with the higher mass gains. X-ray diffraction detected magnetite and haematite on specimens where a mass gain increase was observed and a thick oxide formed. In most cases, the thick oxides were not uniform but formed as nodules, particularly at the corners and edges of the specimens. The thick oxides were not further characterized as they appeared to be consistent with the typical inner spinel-type oxide/outer Fe-rich oxide structure observed on these alloys [21-27].

The STEM characterization focused on the steam exposures at the highest temperature where a protective scale

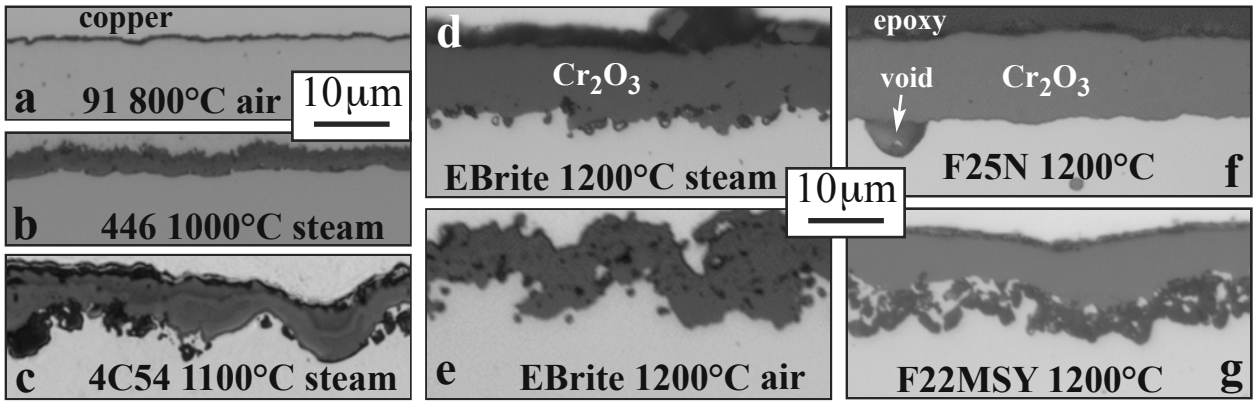

FIGURE 2. Light microscopy of polished sections after 4h exposures (a) Gr.91 at 800°C in air, (b) 446 at 1000°C in steam, (c) 4C54 at 1100°C in steam, (d) Ebrite at 1200°C in steam, (e) EBrite at 1200°C in air, (f) Fe-25Cr (F25N) at 1200°C in steam, and (g) F-22Cr+Mn,Si,Y (F22MSY) at 1200°C in steam

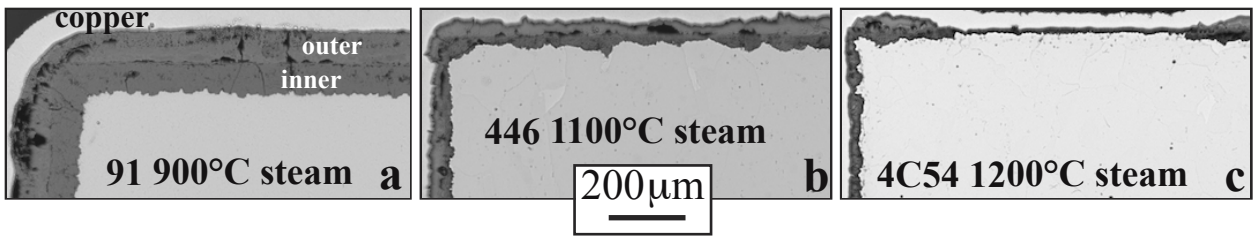

FIGURE 3. Light microscopy of polished sections after 4h exposures in steam (a) Gr.91 at 900°C, (b) 446 at 1100°C and (c) 4C54 at 1200°C.

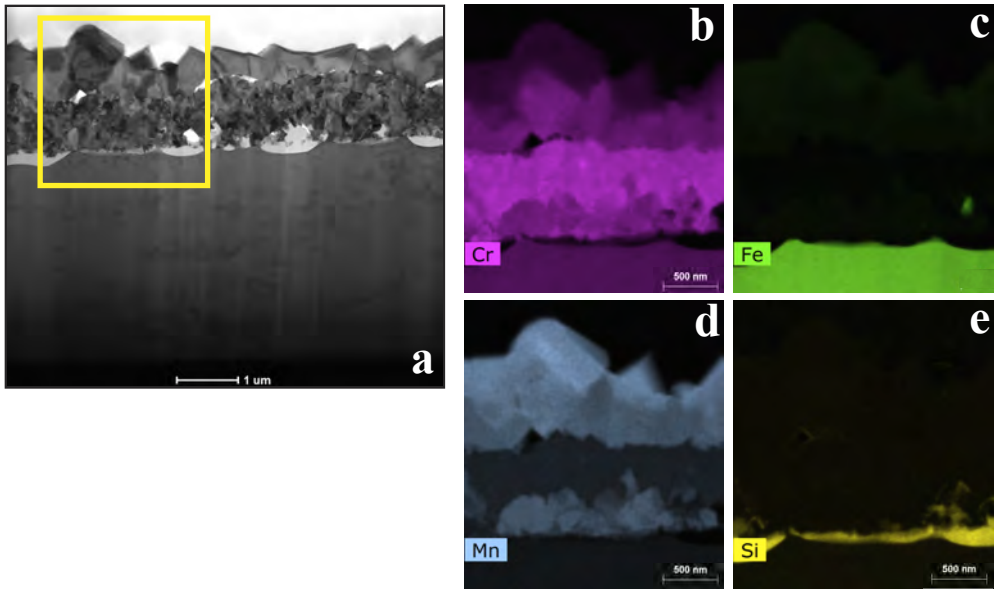

FIGURE 4. (a) STEM bright field image of the scale formed on 446 after 4h at 1000°C and x-ray maps from the box in (a): (b) Cr, (c) Fe (d) Mn and (e) Si

was observed. Figure 4 shows the scale formed on the alloy 446 specimen formed in steam at 1000°C, also shown in Figure 2b. The scale was relatively flat and appeared to consist of multiple layers with the outer layer having the largest grains. The Cr x-ray map in Figure 4b shows that the middle of the oxide is rich in Cr with a fine, nominally equiaxed grain structure slightly elongated in the growth direction. The Mn x-ray map in Figure 4d shows that the outer layer was rich in Mn. However, there was also Mn observed near the metal interface. Both Mn layers contained some Cr and very little Fe, Figure 4c. Figure 4e shows that silica formed at the metal-oxide interface. Selected area diffraction indicated that the silica layer was amorphous. The Mn and Si incorporation in the scale is consistent with the alloy composition, Table 1.

Figure 5a shows the scale formed on the alloy 4C54 specimen after 4h at 1100°C in steam, which also is shown in Figure 2c. In this case, only an outer Mn layer was observed at the gas interface, Figure 5b, with a SiO_2 layer again observed at the metal-oxide interface. A similar structure formed on the 4C54 specimen in air at 1100°C, although the FIB section contained a defect near the metal-oxide interface, Figure 5d. After oxidation in air, the Mn in the scale also was concentrated at the scale-gas interface with some near the defect in the scale, Figure 5e. The O map in Figure 5f shows a difference in O content in the Mn-rich layer and the void in the oxide layer. It is difficult to assess the structure of the defective area and to what degree this area was affected by the FIB milling.

Figure 6 shows images from the scale formed on EBrite in steam at 1200°C. This alloy contains no Mn and a few Si-rich grains were detected near the metal-oxide interface, consistent with the cross-section shown in Figure 2d. The most notable feature of the scale was the incorporation of Fe, Figures 6d and 6h. In the outermost part of the scale, the Fe appeared to be uniformly incorporated in the grain interiors and absent on the oxide grain boundaries, Figure 6d. However, further away from the gas interface in Figure 6a, the Fe was present in Fe-rich oxide precipitates. Near the metal-oxide interface, Fe-rich precipitates also were observed, Figures 6e and 6h. However, in this case they appeared to be metal precipitates and did not appear to contain Cr or O, Figures 6f and 6g.

In order to determine if the Fe incorporation was related to oxidation in steam, the scale formed on EBrite in air at 1200°C also was examined, Figure 7. This scale, which is shown in Figure 2e, also contained Fe in the oxide near the gas interface (Figures 7a and 7b) and Fe-rich oxide precipitates in the middle of the scale (Figures 7c and 7d).

Two model alloys also formed protective oxides in steam at 1200°C. Figure 8 shows the scale formed on the model F25N alloy in steam at 1200°C (Figure 2f). It also contained similar Fe incorporation, transforming from uniform incorporation in the grain interiors near the gas interface (Figures 8a and 8b) to Fe-rich oxide precipitates in the middle of the oxide (Figures 8c and 8d), as was observed on EBrite. Figure 9 shows the oxide formed on Fe-22Cr+Mn,Si,Y (F22MSY). This alloy contained Mn which formed a Mn-rich layer only at the gas interface, Figure 9c, similar to the observation at 1100°C. Rather than forming a silica layer at the metal-oxide interface, discrete SiO_2

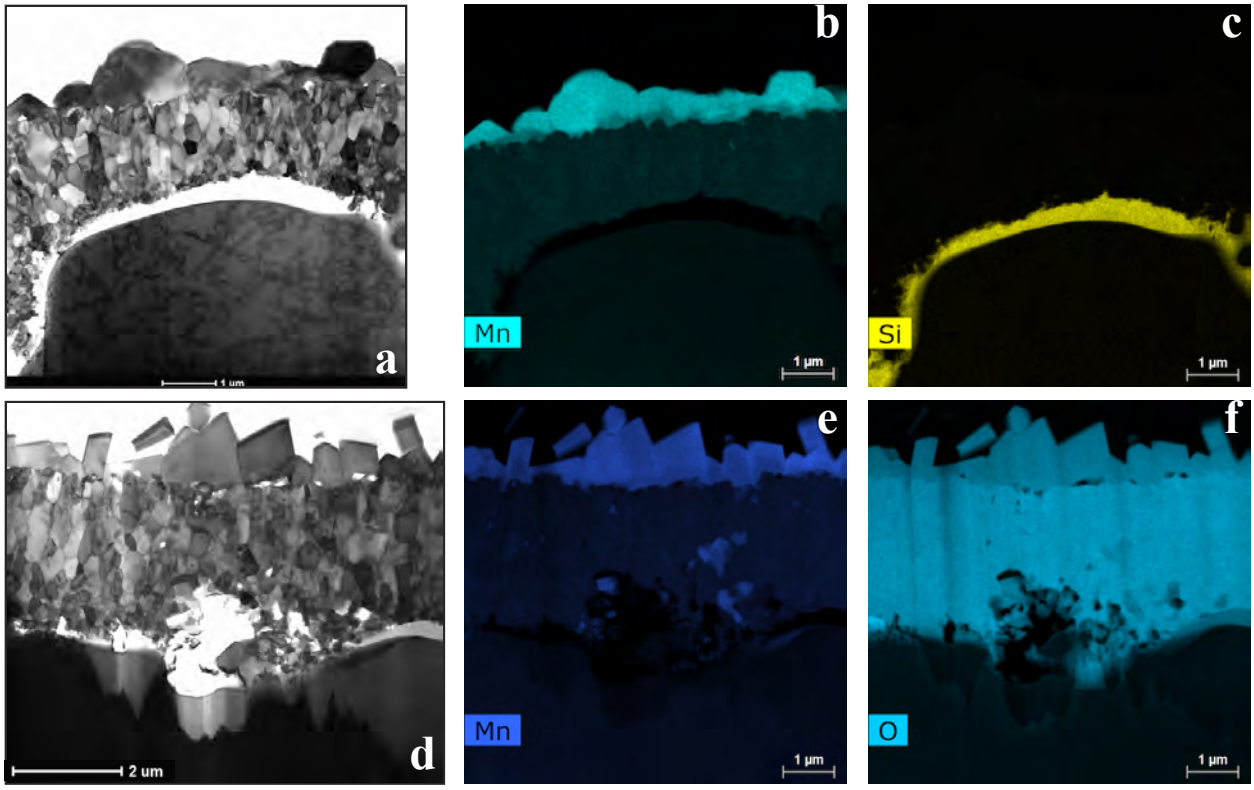

FIGURE 5. STEM analysis of the scale formed on 4C54 at 1100°C (a) bright field STEM image of the scale formed in steam and x-ray maps from (a): (b) Mn and (c) Si; (d) bright field STEM image of the scale formed in air and x-ray maps from (d): (e) Mn and (f) O.

grains were observed in the metal near the reaction front, Figures 9b and 9d. Both electron and x-ray diffraction confirmed that the silica was crystalline (cristobalite) and not amorphous as was observed at 1000° and 1100°C. No Fe-rich oxide or metallic precipitates were observed in the scale formed on this alloy at 1200°C.

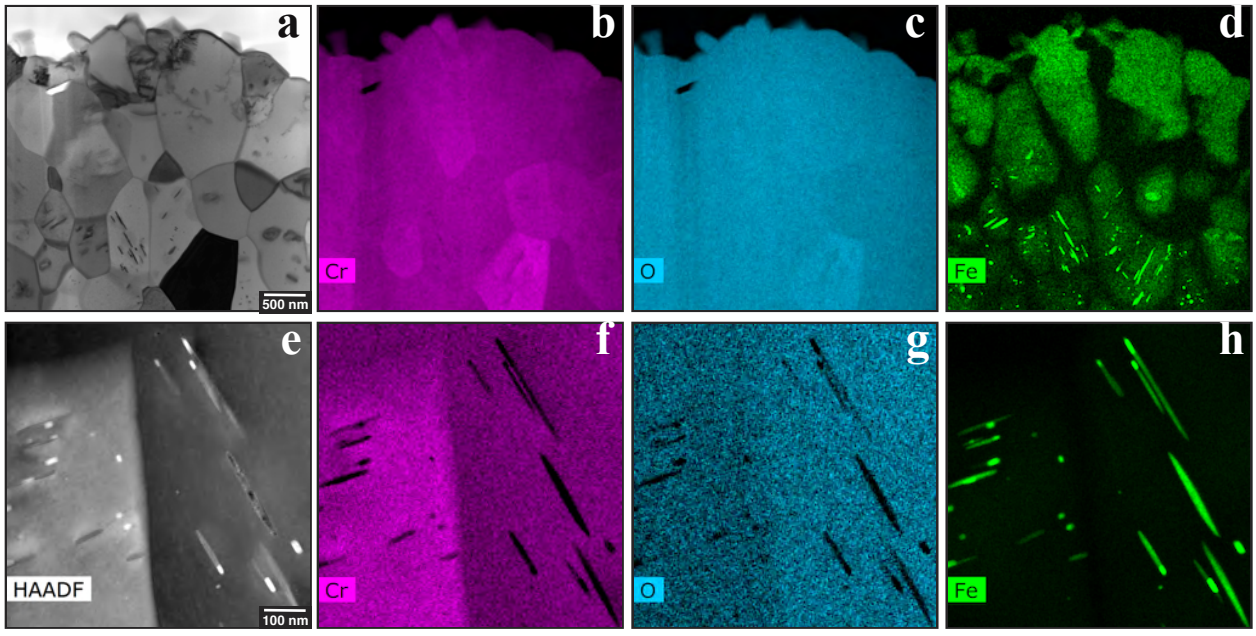

FIGURE 6. (a,e) STEM bright field images of the scale formed on EBrite after 4h at 1200°C in steam and (b-d) x-ray maps from (a) and (f-h) from (e): (b,f) Cr, (c,g) O, and (d,h) Fe. (a) from the gas interface and (e) near the metal interface

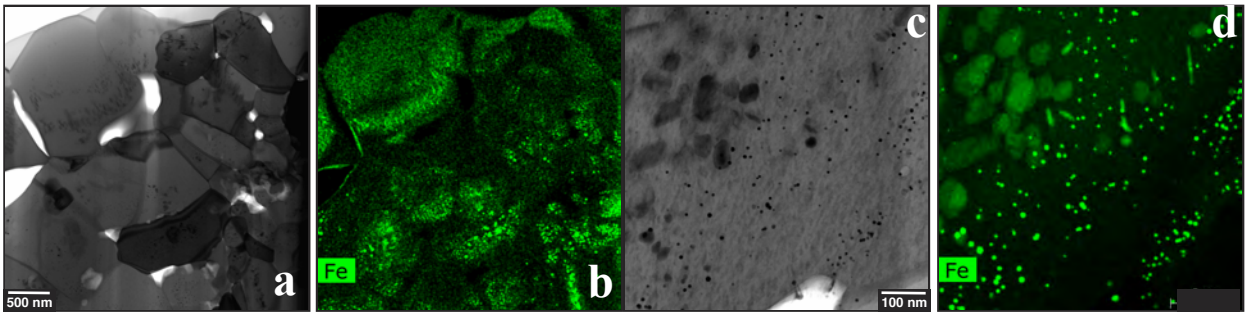

FIGURE 7. (a,c) STEM bright field image of the scale formed on EBrite after 4h at 1200°C in air and Fe x-ray maps (b) from (a) and (d) from (c). (a-b) are near the gas interface and (c-d) are near the center of the scale.

DISCUSSION

The results for the commercial alloys are typical of other studies of the effect of water vapor or steam on the high temperature oxidation of Fe-Cr alloys [13,17,21-27]. Namely, that H_2O reduces the temperature where a given alloy can form a protective scale compared to oxidation in a dry oxidizing environment. The low Cr contents in Grade 91 and 405 were unlikely to form a protective Cr-rich scale at the high temperatures of interest for this application and the formation of a thick Fe-rich oxide in steam is consistent with other studies. The 16.7%Cr in alloy 430 showed very little benefit in terms of increasing the temperature capability, Figure 1.

The most surprising result was that alloys 446 and 4C54 performed significantly worse than EBrite. One contributing factor may be the N content in these alloys, Table 1. If the N ties up Cr in the alloy by forming Cr_2N precipitates, then this Cr is unavailable to support the formation of a protective scale and the Cr content is effectively lower in this alloys. For example, 4C54 has ~0.65at%N, meaning the Cr content is effectively ~1.3at% less. In contrast, the more protective EBrite has a negligible N content. EBrite also has a 1%Mo addition. A previous study of the oxidation of Fe-Cr-Mo and Fe-Cr-W alloys showed that these 5-10 at% additions improved the oxidation resistance of alloys with 9-14%Cr [28].

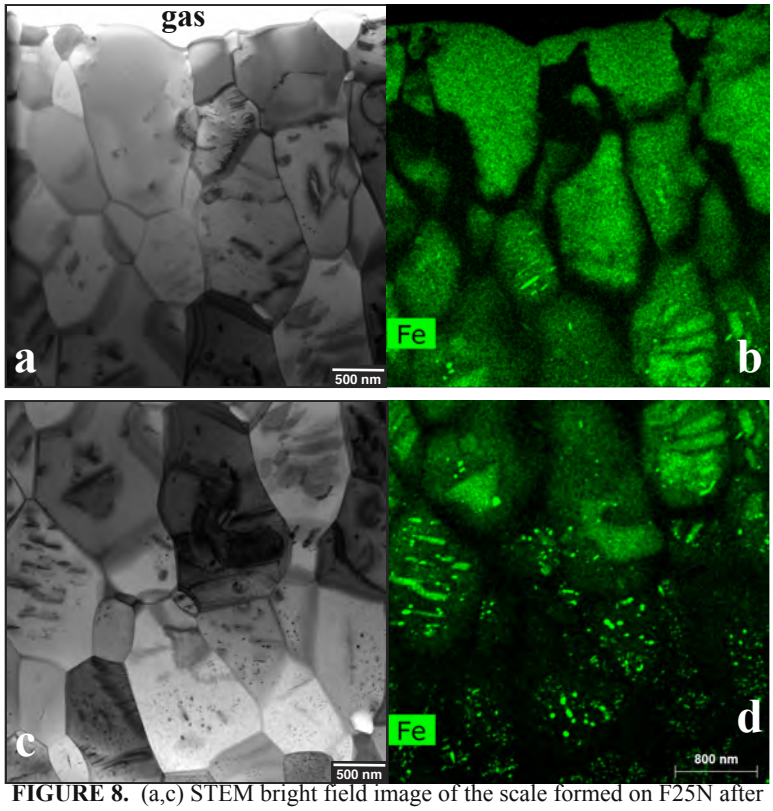

FIGURE 8. (a,c) STEM bright field image of the scale formed on F25N after 4h at 1200°C in steam and Fe x-ray maps (b) from (a) and (d) from (c).

The sensitivity to temperature may also be explained by some of the STEM results. At 1200°C, the silica became crystalline and no longer formed a near continuous layer at the metal-scale interface. Thus, if Si has a beneficial effect on oxidation resistance, this benefit may be limited to temperatures below 1200°C. It is difficult to imagine that the individual SiO_2 crystals yield a protective benefit.

It could be argued that Mn provides some beneficial effect. However, EBrite contains very little Mn and showed the best behavior among the commercial alloys. Also, the model F25N alloy was able to form a protective layer in steam at 1200°C without Mn. It has been widely observed that Mn becomes incorporated into Cr-rich oxides [29]. These results may be slightly different in showing a

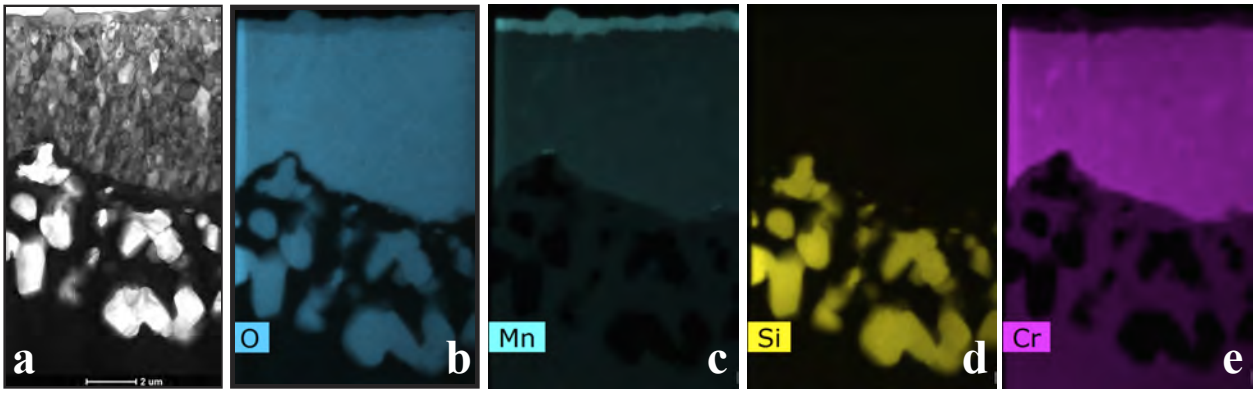

FIGURE 9. (a) STEM bright field image of the scale formed on F22MSY after 4h at 1200°C and x-ray maps from (a): (b) O, (c) Mn, (d) Si and (e) Cr.

layer forming near the metal-oxide interface at 1000°C but not at 1100° or 1200°C, where only a Mn-rich layer was observed at the gas interface. The change with temperature may be due to the rapid diffusion of Mn. MnO is slightly more stable than Cr_2O_3 but less stable than SiO_2, thus it could form between these layers near the metal-oxide interface, where it was observed in Figure 4. However, at higher temperatures the small Mn ion may continue diffusing to the gas interface, much like oxygen-active "reactive" elements diffuse through the scale and become enriched at the gas interface due to the oxygen potental gradient [30,31]. It has been argued that this gas-side Mn-rich layer is beneficial because it inhibits Cr volatilization via $CrO_2(OH)_2$ in the presence of H_2O and O_2. However, in 100% steam, this oxy-hydroxide is unlikely to form with the low O_2 partial pressure and thus this benefit would be absent.

The incorporation of significant Fe in the Cr_2O_3 scale at 1200°C on EBrite and F25N was surprising. The incorporation appeared similar in scales formed in both air and steam although further work is needed to quantify if similar amounts are present in each environment. One might consider this Fe to be detrimental and a precursor to breakaway oxidation, but this was the best performing commercial alloy in the study. The transformation with depth in the scale from near uniform incorporation near the gas interface, to Fe-rich oxide precipitates to metal precipitates near the gas interface may be interpreted by thermodynamics and kinetics. In the Cr_2O_3 scale near the metal-scale interface, the O_2 partial pressure would be sufficiently low to reduce the Fe and form metal precipitates. If the scale is forming by outward or mixed transport, the formation of Fe-rich oxide precipitates may be due to the inner oxide having sufficient time for the nucleation, a process of super-saturation of Fe in the Cr_2O_3 followed by precipitation or a change in Fe solubility with the dropping O_2 partial pressure driving the nucleation. One could also think of an Fe-rich spinel-type oxide initially forming at the gas interface followed by Cr incorporation at the grain boundaries. A time series of observations is needed to better understand how these

It was also surprising that the scale formed on F22MSY contained very little Fe. This could be attributed to an effect of Mn inhibiting Fe incorporation. This hypothesis would explain why very little Fe was incorporated into the scales formed at 1000° and 1100°C. It is possible that the small amount of Y in this alloy affected its performance. However, Y segregation to Cr_2O_3 grain boundaries could not be detected in this alloy, unlike previous Y segregation observations [32]. The unintendedly low Y content may explain the lack of segregation. The Y addition did not reduce the parabolic growth rate by ~10X as might be expected [30]. Nevertheless, more work is needed to determine what inhibits Fe incorporation (e.g. temperature, alloy composition) and if that incorporation affects performance.

Finally, in the context of the fuel cladding application, these results are not particularly promising. It confirmed the prior conclusion [8,9] that ≥25%Cr was needed to form a protective scale at 1200°C in steam. At this level of Cr, the alloy is prone to α′ embrittlement, especially under irradiation [33-37]. This is also an issue for FeCrAl alloys and why alloy development is pushing the Cr content down to 10-13% [12,38]. While E-Brite also was protective at 1300°C in steam, it was not protective at 1400°C. Thus limiting the benefit during the most severe accidents.

SUMMARY

Commercial Fe-Cr alloys were evaluated in 4 h isothermal experiments at 800°-1300°C in steam and air to evaluate their potential as accident tolerant fuel cladding. The alloys were very sensitive to Cr content and only EBrite with

Fe-25.8%Cr-1Mo was able to form a protective scale at 1200°C. Such a high Cr content may be a concern under irradiation in service as a cladding. Characterization of the reaction products formed at 1000°-1200°C by STEM showed several interesting results: (1) a Mn-rich oxide layer formed at both the gas and metal interfaces of the scale at 1000°C but only at the gas interface at 1100° and 1200°C, for steels containing >0.5%Mn, (2) SiO_2 crystallized at 1200°C and no longer formed a layer at the metal-oxide interface and (3) Fe was incorporated in metal and oxide precipitates into protective scales at 1200°C in both steam and air when the alloy did not contain Mn. While more work is needed to fully understand these results, the potential for developing a viable FeCr fuel cladding appears limited.

ACKNOWLEDGMENTS

The experimental work was conducted by M. Howell, M. Stephens, T. Lowe, D. Coffey and T. Jordan. S. Dryepondt and K. Terrani provided useful comments on the manuscript. This research was funded by the U.S. Department of Energy's Office of Nuclear Energy, Advanced Fuel Campaign of the Fuel Cycle R&D program. The FEI Talos F200X STEM was used as part of the Nuclear Science User Facility.

REFERENCES

1. K. R. Robb, M.W. Francis and L. J. Ott, *Nuclear Technology*, **186**, 145 (2014).
2. L. Hallstadius, S. Johnson, E. Lahoda, *Progress in Nuclear Energy*, **57**, 71 (2012).
3. S.J. Zinkle, K.A. Terrani, J.C. Gehin, L.J. Ott, L.L. Snead, *Journal of Nuclear Materials*, **448**, 374 (2014).
4. L. J. Ott, K. R. Robb and D. Wang, *Journal of Nuclear Materials*, **75**, 520 (2014).
5. K. A. Terrani, S. J. Zinkle and L. L. Snead, *Journal of Nuclear Materials*, **448**, 420 (2014).
6. B. A. Pint, K. A. Terrani, Y. Yamamoto and L. L. Snead, *Metallurgical and Materials Transactions* E, **2**, 190 (2015).
7. T. Cheng, J. R. Keiser, M. P. Brady, K. A. Terrani and B. A. Pint, *Journal of Nuclear Materials*, **427**, 396 (2012).
8. B. A. Pint, K. A. Terrani M. P. Brady, T. Cheng and J. R. Keiser, *Journal of Nuclear Materials*, **440**, 420 (2013).
9. B. A. Pint, K. A. Terrani, J. R. Keiser, M. P. Brady, Y. Yamamoto and L. L. Snead, NACE Paper ED2013-3083, Houston, TX, presented at the 16th Environmental Degradation conference, Asheville, NC, August 2013.
10 K. A. Terrani, B. A. Pint, C. M. Parish, C. M. Silva, L. L. Snead and Y. Katoh, *J. Am. Ceram. Soc.*, **97**, 2331 (2014).
11. B. A. Pint, K. A. Unocic and K. A. Terrani, *Materials at High Temperature*, **32**, 28 (2015).
12. Y. Yamamoto, B. A. Pint, K. A. Terrani, K. G. Field, Y. Yang and L.L. Snead, *J. Nuclear Materials*, **467**, 703 (2015).
13. C. T. Fujii and R. A. Meussner, *Journal of the Electrochemical Society*, **111**, 1215 (1964).
14. J. M. Francis and W. H. Whitlow, *Corrosion Science*, **5**, 701 (1965).
15. C. S. Tedmon, *Journal of the Electrochemical Society*, **113**, 766 (1966).
16. G. C. Wood and J. Boustead, *Corrosion Science*, **8**, 719 (1968).
17. G. C. Wood, I. G. Wright, T. Hodgkiess, D. P. Whittle, *Materials and Corrosion*,. **21**, 900 (1970).
18. I. G. Wright and B. A. Wilcox, *Oxidation of Metals*, **8**, 283 (1974).
19. D. Caplan and G. I. Sproule, *Oxidation of Metals*, **9**, 459 (1975).
20. H. Nagai, *Materials Science Forum*, **43**, 75 (1989).
21. J. Shen, L. Zhou and T. Li, *Oxidation of Metals*, **48**, 347 (1997).
22. R. Peraldi and B. A. Pint, *Oxidation of Metals*, **61**, 463 (2004).
23. B. A. Pint and I. G. Wright, *Oxidation of Metals*, **63**, 193 (2005).
24. E. Essuman, G. H. Meier, J. Zurek, M. Hänsel, L. Singheiser and W. J. Quadakkers, *Scripta Materialia*, **57**, 845 (2007).
25. W. J. Quadakkers, J. Żurek, and M. Hänsel, *JOM*, **61** (7), 44 (2009).
26. N. Mu, K. Y. Jung, N. M. Yanar, G. H. Meier, F. S. Pettit, G. R. Holcomb, *Oxidation of Metals*, **78**, 221 (2012).
27. T. Gheno, D. Monceau and D. J. Young, *Corrosion Science*, **64**, 222 (2012).
28. B. A. Pint, B. L. Armstrong, I. G. Wright, M. P. Brady, P. F. Tortorelli, R. R. Judkins and T. R. Armstrong, patent application 12/119,648, submitted 2008, U.S. patent application 2009/0286107, Nov. 19, 2009.
29. W. J. Quadakkers, J. Piron-Abellan, V. Shemet and L. Singheiser, *Materials at High Temperature*, **20**, 115 (2003).
30. B. A. Pint, *Oxidation of Metals*, **45**, 1-37 (1996).
31. B. A. Pint, A. J. Garratt-Reed and L. W. Hobbs, *Journal of the American Ceramic Society*, **81**, 305 (1998).
32. C. M. Cotell, G. J. Yurek, R. J. Hussey, D. F. Mitchell and M. J. Graham, *Oxidation of Metals*, **34**, 173 & 201 (1990).
33. T. Denys and P. M. Gielen, *Metallurgical Transactions* **2**, 1423 (1971).
34. P. J. Grobner, *Metallurgical Transactions*, **4**, 251 (1973).
35. F. Danoix, P. Auger, *Materials characterization* **44**, 177 (2000).
36. G. Bonny, D. Terentyev, L. Malerba, *Journal of phase equilibria and diffusion*, **31**, 439 (2010).
37. M. H. Mathon, Y. de Carlan, G. Geoffroy, X. Averty, A. Alamo and C. H. de Novion, *J. Nucl. Mater.*, **312**, 236 (2003).
38. K. G. Field, X. Hu, K. Littrell, Y. Yamamoto and L. L. Snead, *Journal of Nuclear Materials*, **465**,746 (2015).